Redox Biology 37 (2020) 101676

Contents lists available at ScienceDirect

Redox Biology

journal homepage: www.elsevier.com/locate/redox

Research Paper

A new target for an old DUB: UCH-L1 regulates mitofusin-2 levels, altering mitochondrial morphology, function and calcium uptake

Fernanda M. Cerqueira [a,b,c], Sophia von Stockum [c], Marta Giacomello [c,d], Inna Goliand [b], Pamela Kakimoto [e], Elena Marchesan [c], Diego De Stefani [d], Alicia J. Kowaltowski [e], Elena Ziviani [c], Orian S. Shirihai [a,f,*]

[a] Obesity Research Center, Molecular Medicine, Boston University School of Medicine, Boston, MA, 02111, USA
[b] National Institute for Biotechnology in the Negev, Ben Gurion University, Beer-Sheva, 8410501, Israel
[c] Department of Biology, University of Padua, Padua, 35121, Italy
[d] Department of Biomedical Sciences, University of Padua, 35121, Italy
[e] Departmento de Bioquímica, Instituto de Química, Universidade de São Paulo, São Paulo, 05508-900, Brazil
[f] UCLA Section of Endocrinology, Department of Medicine, David Geffen School of Medicine, UCLA, CA, 9095-7073, USA

ARTICLE INFO

Keywords:
Parkinson's disease
Mitochondrial function
Deubiquitinase
Mitochondria

ABSTRACT

UCH-L1 is a deubiquitinating enzyme (DUB), highly abundant in neurons, with a sub-cellular localization dependent on its farnesylation state. Despite UCH-L1′s association with familial Parkinson's Disease (PD), the effects on mitochondrial bioenergetics and quality control remain unexplored. Here we investigated the role of UCHL-1 in mitochondrial dynamics and bioenergetics. We demonstrate that knock-down (KD) of UCH-L1 in different cell lines reduces the levels of the mitochondrial fusion protein Mitofusin-2, but not Mitofusin-1, resulting in mitochondrial enlargement and disruption of the tubular network. This was associated with lower tethering between mitochondria and the endoplasmic reticulum, consequently altering mitochondrial calcium uptake. Respiratory function was also altered, as UCH-L1 KD cells displayed higher proton leak and maximum respiratory capacity. Conversely, overexpression of UCH-L1 increased Mfn2 levels, an effect dramatically enhanced by the mutation of the farnesylation site (C220S), which drives UCH-L1 binding to membranes. These data indicate that the soluble cytosolic form of UCH-L1 regulates Mitofusin-2 levels and mitochondrial function. These effects are biologically conserved, since knock-down of the corresponding UCH-L1 ortholog in *D. melanogaster* reduces levels of the mitofusin ortholog Marf and also increases mitochondrial respiratory capacity. We thus show that Mfn-2 levels are directly affected by UCH-L1, demonstrating that the mitochondrial roles of DUBs go beyond controlling mitophagy rates.

1. Introduction

Parkinson's disease (PD) is the second most common age-related neurodegenerative disorder worldwide, characterized by loss of dopaminergic neurons and neuronal Lewy body inclusions. Although most PD cases are sporadic, many insights into the disease process came from research of genes associated to familial PD [1], named collectively PARK (Parkinson disease associated genes) and numbered from 1-18 [2]. Studies on alpha-synuclein mutations have demonstrated that alpha-synuclein misfolding, aggregation and associated mitochondrial dysfunction are at the center of PD's progression in familial and sporadic cases [3–5]. Other PARK genes directly associated to mitochondrial dysfunction are PRKN (Parkin RBR E3 ubiquitin protein ligase), PINK1 (PTEN-Induced Putative Kinase Protein 1) and DJ-1 (Parkisonism associated deglycase) [6]. The investigation of the phenotypes caused by mutations or lack of these genes have revealed their central role in mitophagy and overall mitochondrial quality control [7–10].

Parkin is a ubiquitin E3 ligase, part of the UPS (ubiquitin-proteasome system), which was found to be a major regulator of mitophagy, through ubiquitination of outer-mitochondrial membrane proteins, regulating their degradation [11]. The cross-talk between the UPS and mitochondrial function plays a major role in cellular homeostasis [12,13]. The only other UPS protein known to be linked to PD is Ubiquitin C-terminal hydrolase L-1 (UCH-L1), coded by a gene classified as PARK 5 [2,14]. Contrary to Parkin, UCH-L1 acts as a deubiquitinating enzyme, recycling

* Corresponding author. UCLA Section of Endocrinology, Department of Medicine, David Geffen School of Medicine, UCLA, CA, 9095-7073, USA.
E-mail address: OShirihai@mednet.ucla.edu (O.S. Shirihai).

https://doi.org/10.1016/j.redox.2020.101676
Received 18 May 2020; Received in revised form 13 July 2020; Accepted 3 August 2020
Available online 7 August 2020

Abbreviation list

AEQ	Aequorine
CFP	Cyan fluorescent protein
DUB	Deubiquitinase
ER	Endoplasmic reticulum
ERMICC	ER-mitochondria contact efficiency
FCCP	Carbonyl cyanide-4-(trifluoromethoxy)phenylhydrasone
FEMP	FRET-based indicator of ER–mitochondria proximity
FKBP	FK506 binding protein
FRB	FKBP-rapamycin-binding (FRB) domain
FRET	Fluorescence resonance energy transfer
KD	Knock-down
NADH	Nicotinamide adenine dinucleotide
Mfns	Mitofusins
Mfn-2	Mitofusin-2
OCR	Oxygen consumption rates
OMM	Outer mitochondrial membrane
PARK	Parkinson disease associated genes
PD	Parkinson's disease
PINK-1	PTEN-Induced putative kinase protein 1
UCH-L1	Ubiquitin C-terminal hydrolase L-1
UCH	Ubiquitin carboxyl hydrolase
UPS	Ubqiuitin-proteasome system
USP	Ubiquitin-specific peptidase
VDAC	Voltage-dependent anion channel
WT	Wild type
YFP	Yellow fluorescent protein

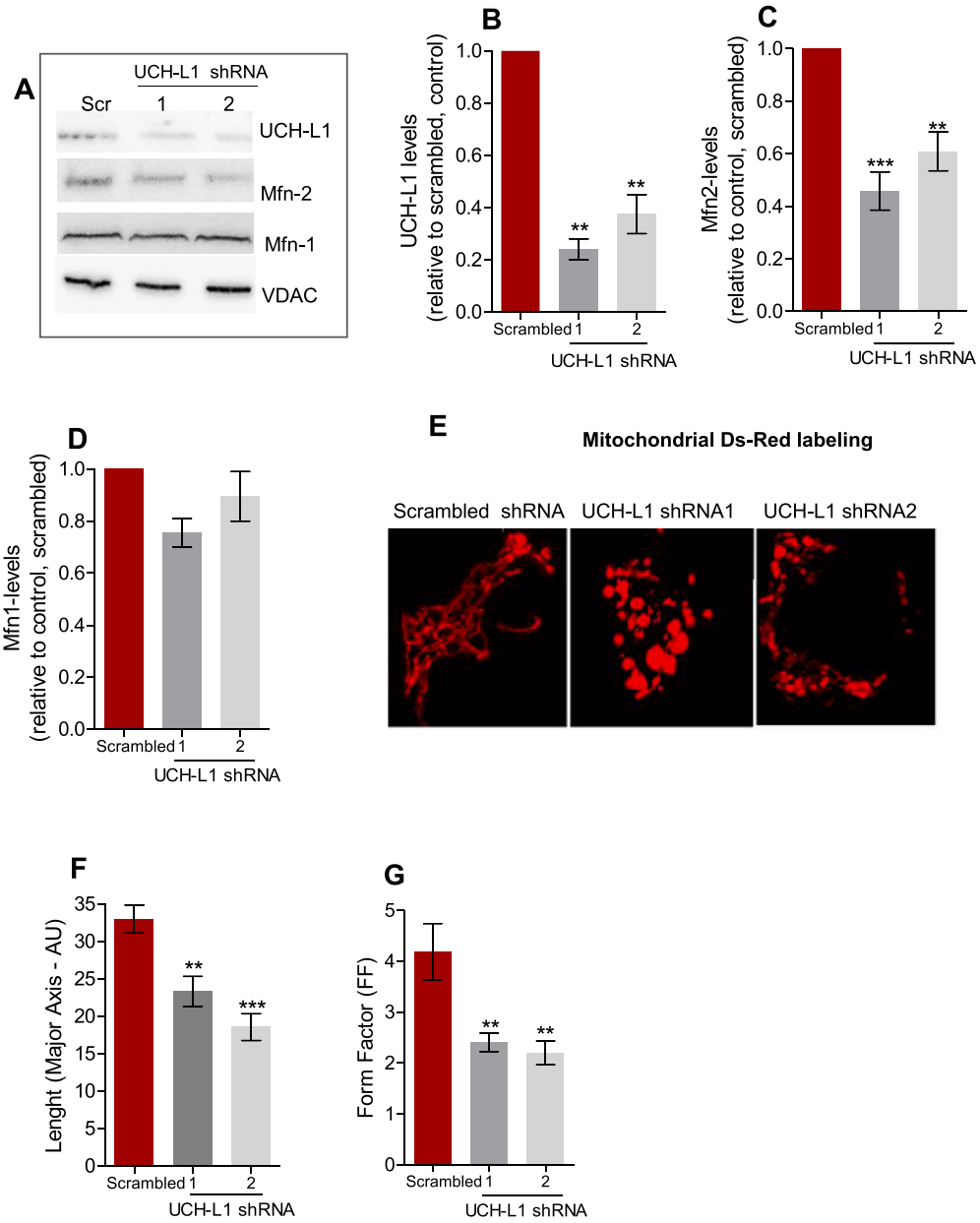

Fig. 1. UCH-L1 knockdown reduces Mfn2, but not Mfn1, altering mitochondrial morphology. Representative blots of UCH-L1, Mfn1, Mfn2 and VDAC from neuroblastoma SH-SY5Y cells of the indicated genotype, quantified in (B), (C), and (D), respectively. VDAC was used as loading control. (E) Representative confocal images of SH-SY5Y cells of the indicated genotype, co-transfected with mitochondrial Ds-Red. Scale bars, 5 μM. (F) length of mitochondrial structures. (G) Form Factor morphology analysis and $^{**}p < 0.01$ *vs.* scrambled; $^{***}p < 0.001$ vs. scrambled. (For interpretation of the references to colour in this figure legend, the reader is referred to the Web version of this article.)

free ubiquitin [15,16]. Moreover, 30% of UCH-L1 is farnesylated and associated to membranes, and this form was found to raise intracellular levels of alpha-synuclein [17]. UCH-L1 is very abundant in neurons, comprising up to 2% of the total protein [18,19], and its levels are regulated by Parkin, which ubiquitinates UCH-L1, targeting it to degradation [20]. Despite UCH-L1′s direct interaction with Parkin and alpha-synuclein, major role in UPS, and link to familial PD, its mitochondrial effects remain unknown. Addressing this gap can provide a new connection between the UPS and mitochondrial function, and ultimately retrieve new pathways for interventions in PD and other chronic diseases.

In this study we report for the first time that UCH-L1 is involved in the regulation of mitochondrial morphology and, consequently, function. We identified Mfn2 as an OMM UCH-L1 target: its protein levels positively correlate with UCH-L1 content in neuroblastoma SH-SY5Y cells, immortalized beta-cell INS1 and *Drosophila melanogaster*. Knocking-down UCH-L1 results in enlarged mitochondria, with lower mitochondria-ER contact sites, reduced mitochondrial Ca^{2+} uptake and altered mitochondrial network and oxygen consumption rates. Consistently, the overexpression of UCH-L1 increases Mfn2 levels and this effect is strikingly enhanced by the mutant form, which lacks the farnesylation site (UCH-L1^{C220S}), and is unable to bind membranes, implying a specific role for the cytosolic form of UCH-L1 in shaping mitochondrial physiology.

2. Results and discussion

2.1. Loss of UCH-L1 reduces Mfn-2 levels and mitochondrial connectivity

Two different shRNAs (1 and 2) were used to silence UCH-L1 in neuroblastoma SH-SY5Y cells. Their respective knock-down (KD) efficiency was of approximately 62.5 ± 0.4% and 76 ± 0.75% (Fig. 1 A, B). In both cases, we observed alterations in mitochondrial morphology. While the control (scrambled shRNA) cells presented a tubular mitochondrial network, UCH-L1 KD shortened the length of the connected structures (Fig. 1 E, F), as well as lowered branching, measured by the form factor (Fig. 1 G), which takes into account the length and the area of mitochondrial structures [21]. These effects were associated with a

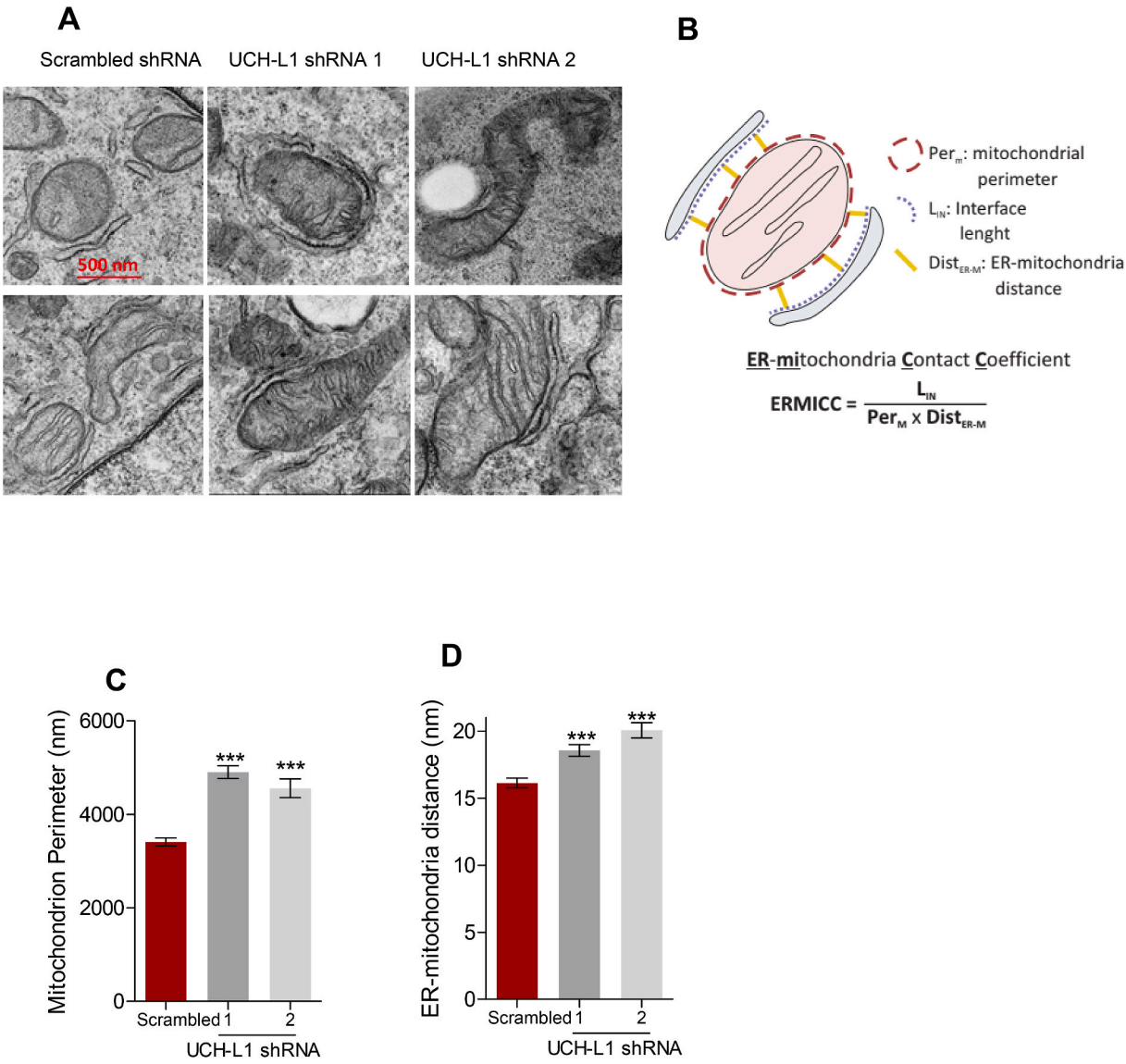

Fig. 2. UCH-L1 ablation results in mitochondrial enlargement and increases ER–mitochondria distance. (A) Representative EM images of SH-SY5Y cells of the indicated genotype. (Scale bars, 500 nm) (B) A schematic view of the structures analyzed for the ER-mitochondria distance calculation and ERMICC contact index. (C) Mean ± SEM of mitochondrial perimeter (D) Mean ± SEM of ER-mitochondria distance (E) Mean ± SEM of ERMICC index. Three independent experiments were performed and 40–100 images per condition were taken in each experiment. ***$p < 0.001$ *vs.* scrambled.

significant reduction in Mfn2 protein levels (54.15 ± 0.18% and 30.02 ± 0.18%, respectively), but not Mnf1 (Fig. 1A,C and D). The use of the proteasome inhibitor MG-132 prevented the reduction in Mfn2 levels (Supplementary Fig. 1). In fact, MG-132 increased Mfn-2 levels in both control (scrambled shRNA) and UCH-L1 KD groups. Pharmacological proteasome inhibition is known to increase the levels of several mitochondrial proteins, recycled by this system [22,23].

UCH-L1 effects on mitochondrial morphology and Mfn2 levels were reproduced in immortalized INS1 beta-cells (Supplementary Fig. 2), which share many similarities with neurons, despite their different embryological origins [24]. A large group of neuronal markers is expressed in beta-cells, including Parkin [25] and UCH-L1 [26].

Electron microscopy confirmed altered mitochondrial morphology as a result of UCH-L1 ablation (Fig. 2). Mitochondrial units were enlarged in SH-SY5Y cells with UCH-L1 KD compared to scrambled control (Fig. 2 A, C); a similar alteration has been reported in Mfn2 knockout (KO) cardiomyocytes [27]. Interestingly, looking at the mitochondrial network imaged by confocal microscopy (Fig. 1, Supplementary Fig. 2), the diameters of some of the spherical mitochondria in both SH-SY5Y and INS1 cells with UCH-L1 KD cells are significantly larger than the diameters of mitochondrial structures in scrambled cells. This specific alteration was first reported by Chen et al.. [2003; 28] in Mfn2-deficient MEF cells, emphasizing the role of Mfn2 for tubular shape maintenance.

Although a number of mitochondrial proteins are ubiquitinated [23], Mitofusins (Mfns) have been most extensively studied due to their involvement in the mitophagy pathway mediated by Pink1/Parkin [11,22,29,30]. It is well known that Mfns shape mitochondrial morphology and, therefore, fate [28,31–34], and their levels were recently shown to be regulated by mammalian DUBs which oppose mitophagy: USP30, USP35, USP15, and USP14 [35–38].

2.2. UCH-L1 ablation disrupts mitochondrial-ER tethers and reduces Ca^{2+} uptake

A small area of the outer mitochondrial membrane (OMM), around 12–20%, depending on the cell type, is estimated to be associated with the ER, at a distance of 10–50 nm, which enables ER and OMM protein complexes to directly interact [39,40]. The physical distance between both organelles was significantly increased by the KD of UCH-L1 (Fig. 2 A, D) and the interface area within the tether range was significantly reduced, resulting in a lower ER-mitochondria contact efficiency (ERMICC, Fig. 2 B, E).

Another approach to investigate ER–mitochondria physical tethering was performed, using the FRET-based indicator of ER–mitochondria proximity (FEMP) where FRET changes are proportional to the extent and number of contacts between the two organelles [41,42]. During translation, the FEMP polypeptide undergoes autocleavage and releases YFP and CFP targeted to different organelles (OMM and ER, respectively). Between the fluorescent probe and the localization signal, one of the components of the Rapamycin-heterodimerization system is located (FKBP and FRB, respectively) [41,42]. Addition of rapamycin causes heterodimerization between adjacent FKBP and FRB domains to rapidly connect the ER- and OMM-targeted anchors (Supplementary Fig. 3 A, B, C) [41,42].

Thus, maximization of the FRET ratio (FRET after rapamycin/FRET before rapamycin) signal, confined to the areas where the ER and OMM are naturally close (Supplementary Figure 3 A), was significantly reduced by both UCH-L1 KDs (Supplementary Figure 3 D), providing further evidence that UCH-L1 impacts ER-mitochondria tethering.

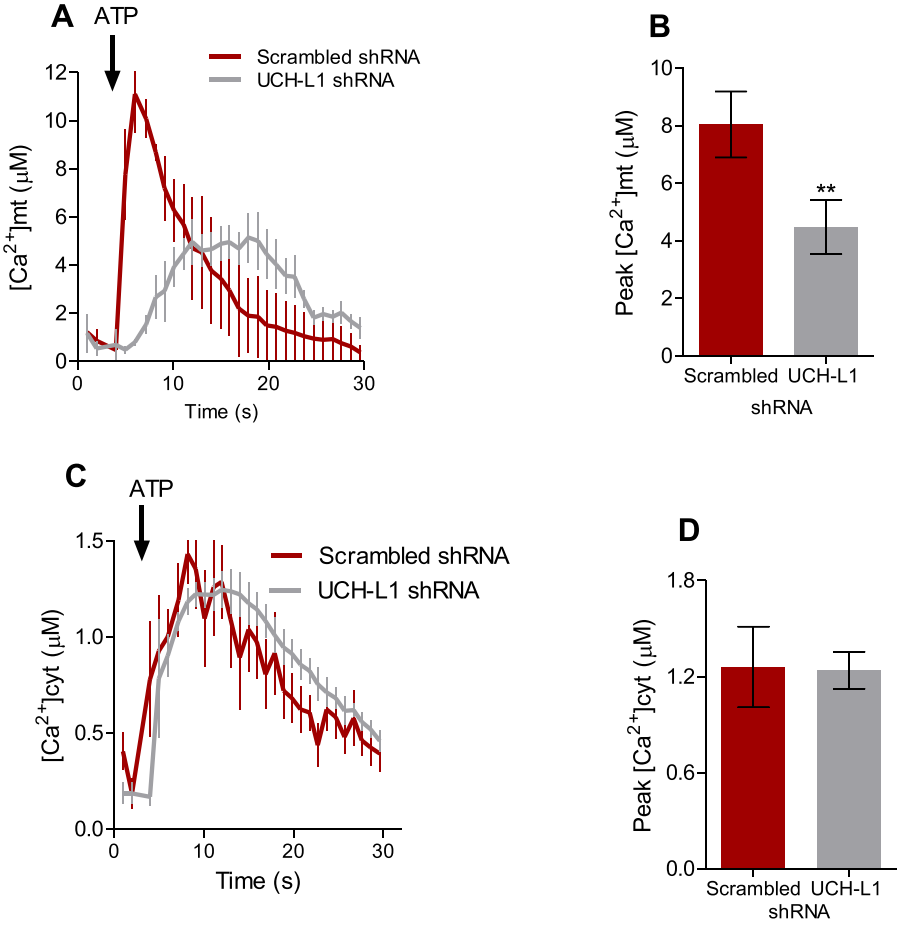

Fig. 3. UCH-L1 ablation decreases mitochondrial Ca^{2+} uptake *in vitro*. SH-SY5Y cells stably expressing scramble or UCH-L1 shRNA were infected with cytAEQ or mtAEQ. (A) Time-response raise in mitochondrial Ca^{2+} concentrations ($[Ca^{2+}]_{mt}$) in response to ATP (0.2 mM) in Ca^{2+}-free Krebbs Ringer buffer (KRB). Peak of ($[Ca^{2+}]_{mt}$) (Mean ± SEM) analyzed in (B). (C) Time-response raise in cytosolic Ca^{2+} concentrations ($[Ca^{2+}]_{cyt}$) in response to ATP (0.2 mM) in Ca^{2+}-free Krebbs Ringer buffer (KRB). Peak of $[Ca^{2+}]$cyt (Mean ± SEM) analyzed in (D). Results from 5 independent experiments (n = 3–6 recordings per experiment). $^{**}p < 0.01$ *vs.* scrambled.

The diminished interaction between both organelles was further corroborated by the lower mitochondrial calcium uptake in response to ATP (Fig. 3 A, B), without any effect in cytosolic calcium (Fig. 3 C, D), measured by mitochondrial and cytosolic Aequorine, respectively. Although the Mfn2 role in the tethering between both organelles is controversial, with some studies demonstrating Mfn2 enhances the tethering [42–44], while others report the opposite effect [45,46], the seminal role of Mfn2 in the communication between the ER and mitochondria is mostly well-acknowledged. Moreover, changes in mitochondrial morphology *per se* were shown to disrupt the communication between both organelles [47].

2.3. UCH-L1 KD increases mitochondrial OCR and mitochondrial complex I activity

UCH-L1 KD resulted in overall higher mitochondrial oxygen consumption rates (OCR) in SH-SY5Y neuroblastoma cells (Fig. 4): Basal OCR was significantly increased (Fig. 4 A, B), which can be the result of a higher proton leak (Fig. 4 A, D), normally associated to a higher electron flow in the respiratory chain [48–50]. Despite increased leakage, the overall enhancement in OCR was associated to a higher mitochondrial ATP production in absolute values (Fig. 4 A, C). The maximum OCR, recorded in the presence of an uncoupling agent, in this study FCCP, allows oxygen consumption to be independent of the ATP synthesis, and provides a measurement known as "mitochondrial spare capacity", was significantly augmented in UCH-L1 KD cells (Fig. 4 A, E).

Many factors can affect the mitochondrial spare capacity, including activities of the respiratory complexes [51]. Mitochondrial complex I activity in cell lysates, measured by following NADH oxidation spectrophotometrically, was 2.5 fold higher in UCH-L1 KD SH-SY5Y cells compared to control (scrambled) cells (Fig. 5 A, B), while no differences were observed in Complex II (0.67 ± 0.37 μM sec^{-1} for UCH-L1 KD vs. 0.51 ± 0.09 μM sec^{-1} for scramble cells). Metabolites present in the cell culture media may determine which complex activities are preferably modulated [52].

The regulation of mitochondrial function by DUBs has not being described yet. On the other hand, metabolic changes in response to Mfn2 levels have being extensively studied (reviewed in Ref. [53,54] and were shown to differ between tissues and cells types. While some studies associated lower OCRs with reduced Mfn2 content [33,55], we and others have demonstrated that reduction in Mfn2 content result in higher OCRs [56,57].

2.4. Cytosolic localization and DUB activity are necessary for UCH-L1 regulation of Mfn2 levels

Overexpression of wild type UCH-L1 (UCH-L1^{WT}) significantly augmented the levels of Mfn2, and this effect was strikingly enhanced by a mutation in the farnesylation site (C220S) (Fig. 6), impairing the protein ability to bind to membranes [17]. Increasing the availability of cytosolic UCH-L1 (UCH-L1^{C220S}) raised Mfn2 protein levels 2.5 times compared to the vector plasmid, and 1.5 times compared to UCH-L1^{WT} (Fig. 6 A, B, C), also observed by immunohistochemistry (Fig. 6 D, E). Taken together, these results further corroborate the role of UCH-L1 in regulating Mfn2 content.

Although a significant portion of UCH-L1 is bound to the ER membrane [17] and, therefore, could potentially interact with Mfn-2 at the tether site, our results demonstrate that the cytosolic form of UCH-L1 is

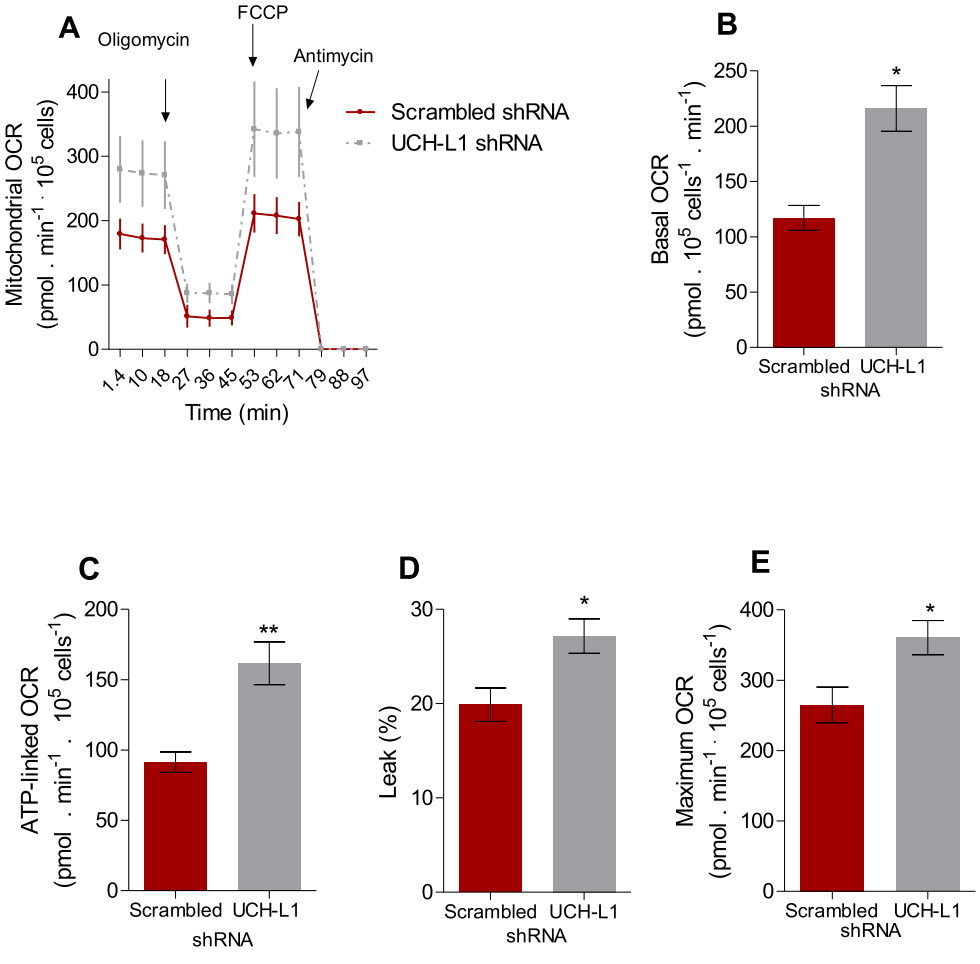

Fig. 4. UCH-L1 ablation increases mitochondrial oxygen consumption rates (mtOCR). (A) Representative mitochondrial oxygen consumption rates (OCR) of neuroblastoma SH-SY5Y cells stably expressing scrambled or UCH-L1 shRNA under basal conditions and after the subsequent addition of 2 μM oligomicin, 5 μM FCCP and 2 μM antimycin. (B) Basal mtOCR; (C) ATP-linked mtOCR (basal mtOCR minus oligomycin-insensitive-mtOCR); (D) % of mitochondrial leak (E) maximal mtOCR (highest OCR after FCCP addition). OCR values in the presence of antimycin (non-mitochondrial respiration) were subtracted from all quantifications. Results from 3 independent experiments, $^{*}p < 0.05$ *vs.* DMSO. $^{**}p < 0.01$ *vs.* scrambled.

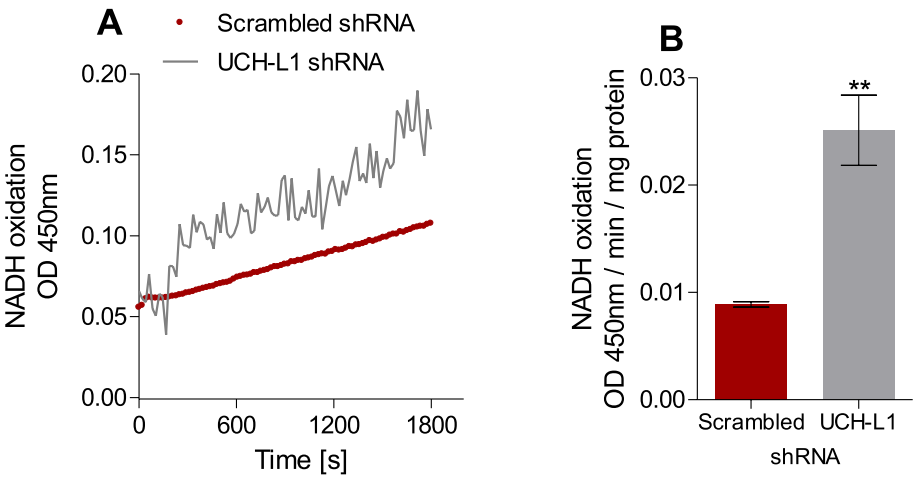

Fig. 5. UCH-L1 ablation increases mitochondrial Complex I activity. (A) Representative traces of NADH oxidation by mitochondria from SH-SY5Y cells stably expressing scramble or UCH-L1 shRNA. (B) Complex I activity expressed in OD · min^{-1} · mg of $protein^{-1}$. $^{**}p < 0.01$ *vs.* scrambled.

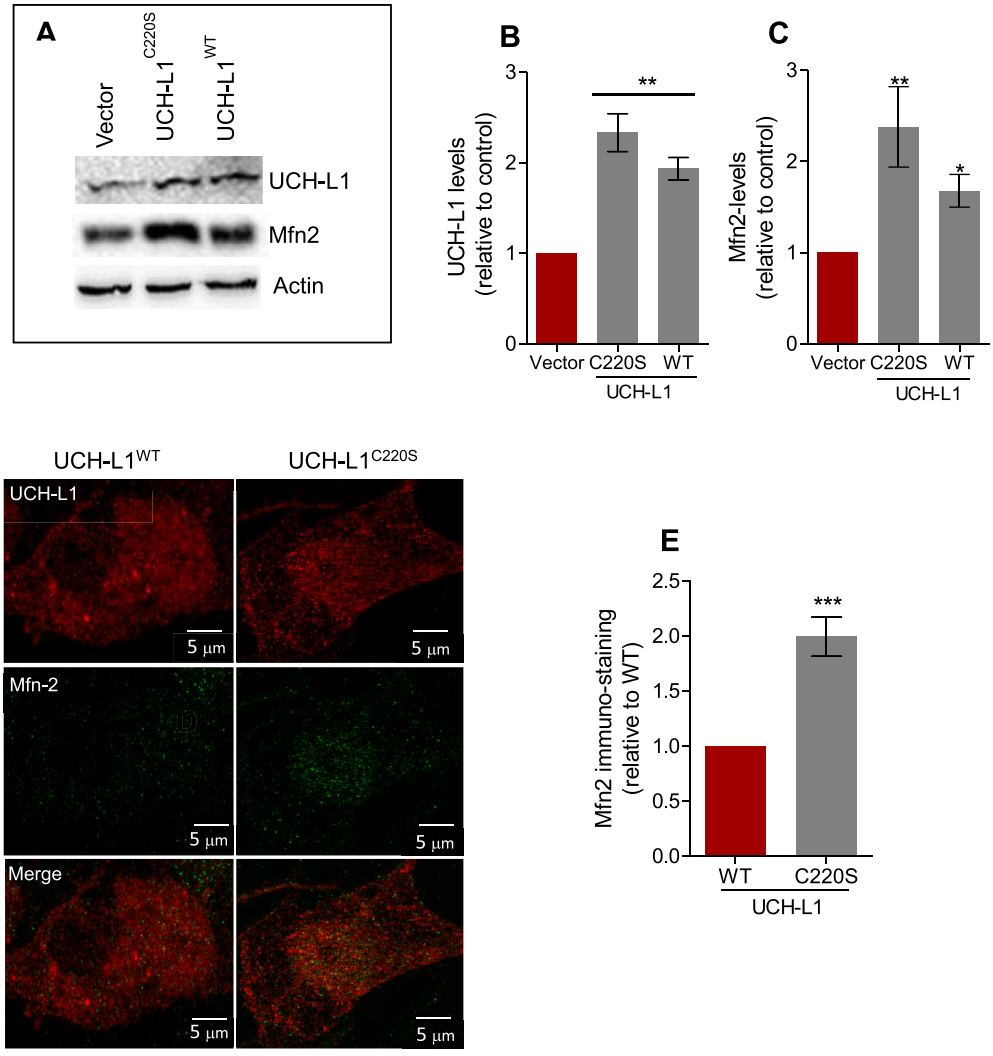

Fig. 6. Farnesylation determines UCH-L1 effects on Mfn2 levels. (A) Representative blots of UCH-L1 and Mfn2 from neuroblastoma SH-SY-5H cells of the indicated genotype, quantified in (B) and (C), respectively. Actin was used as loading control. (D) High resolution maximum intensity projection of neuroblastomas SH-SY5H of the indicated genotype immunostained for Mfn-2 (green) and UCH-L1 (red). Cells were imaged using SIM. (E) Maximum Intensity Fluorescence was calculated in Image J. $^{*}p < 0.05$ *vs.* vector; $^{**}p < 0.01$ *vs.* vector; $^{***}p < 0.001$ *vs.* WT. (For interpretation of the references to colour in this figure legend, the reader is referred to the Web version of this article.)

exerting a role in the regulation of Mfn2 levels. Whereas the access of folded proteins to UCH-L1 enzymatic pocket is restricted [58,59]), it has been hypothesized that the binding of the correct substrate can induce the juxtaposed regions to extend, acquiring an accessible conformation.

In vitro studies have shown that UCH-L1 cleaves ubiquitin efficiently from C-terminal extensions [58], as well as hydrolyses K-63 poly-ubiquitin chains in alpha-synuclein, and alternatively ubiquitinates alpha-synuclein when dimerized [60]. UCH-L1 was also shown to cleave

N-terminal-linked mono-ubiquitin [61] and to stabilize mono-ubiquitin in proteins [62]. Interestingly, Mitofusins have been reported to be mono-ubiquitinated [11,29].

2.5. UCH KD reduces marf levels and increases maximum mtOCR in Drosophila melanogaster

D. melanogaster has been widely used to study the roles of ubiquitin ligases and DUBs in the regulation of mitochondrial quality control [63,64] and relevant PD models were developed by manipulating proteins involved in this process [65]. UCH (Ubiquitin Carboxyl Terminal Hydrolase) is the *Drosophila melanogaster* ortholog of human and mouse UCH-L1 [66]. The whole-body Knock-down (KD) of UCH substantially decreased levels of the Mfn homologue in flies, Marf (Fig. 7A). Isolated mitochondria from UCH KD flies displayed higher oligomycin-insensitive and significantly higher maximum OCR compared to mitochondria isolated from control, Actin Gal 4, flies (Fig. 7B), following the same patterns observed in the mammalian SH-SY5Y. In isolated mitochondria, maximum OCR may reflect differences in super-complex content, activity and assembly, NAD^+ availability, membrane composition, levels and activity of proteins of the respiratory chain, and many other effects [51,67,68]. In intact cells, mitochondrial morphology is also an important determinant factor of OCR [50]. In SH-SY5Y, all OCR values were increased, however, during the isolation process, mitochondrial morphology is disrupted and, therefore, not all OCR changes observed in intact cells will be reproduced in isolated mitochondria.

Neuronal abundance and the involvement of UCH-L1 in the UPS suggest that changes in its content may alter the homeostasis of proteins degraded by the proteasome and impact several cellular pathways. Many DUBs exist in an "inactive state" that requires interaction with other molecules or post-translational modifications to acquire an "active" conformation, avoiding aberrant activity, not desirable for proteins with a regulatory role, especially highly abundant proteins [69]. The multiple post-translational modifications UCH-L1 can have are likely the answer for the apparent divergence between its high abundance and low enzymatic activity from *in vitro* assays. Studying UCH-L1 in a cellular context may retrieve new targets for this DUB.

The identification of Mfn2 as a protein which responds to UCH-L1 levels, *in vivo* and *in vitro*, tightens the gap between the UPS and mitochondrial quality control. Stabilization of Mfn2 levels was shown to prevent the loss of dopaminergic neurons in cellular models of PD [70,71]. The overexpression of UCH-L1 was previously associated with proteasome inhibition [17], which should be taken into consideration in the interpretation of the overexpression results. However, the KD studies in mammalian cell lines and *D. melanogaster* support the idea that UCH-L1 has a seminal role in the regulation of Mfn2 levels. Although UCH-L1 KD does not cause a full loss in Mfn2 content, the resulting phenotype resembles what was previously described in Mfn2-deficient models [28,57]. Additional studies are required to determine if Mfn2 is a direct substrate of UCH-L1, and what cellular signals trigger this interaction, or if UCH-L1 targets another "Mfn2 regulatory protein". Nonetheless, the mitochondrial changes in response to UCH-L1 are a proof of concept that DUBs regulate mitochondrial physiology beyond mitophagy.

3. Methodology

3.1. Plasmids, lentivirus and cell culture

SH-SY5Y cells stably expressing UCH-L1 or scrambled shRNA were obtained by lentivirus infection. Briefly, HEK293T cells were transfected with scrambled or UCH-L1 –GFP-shRNAs, both vectors containing puromycin resistance sequence (Applied Biological Materials, Richmond, BC, Canada) and co-transfected with packing and envelop vectors, PAX2 and PM2.G (Addgene, Watertown, MA) respectively, using Lipofectamin 2000 (Invitrogen) diluted in Opt-MEM reduced serum media (Thermo Fisher). After 48 h, the cell media were collected and the crude extract used to infect SH-SY5Y cells. After 24 h, GFP positive signal was used to confirm the infection efficiency and after 48 h, the highly GFP-expressing cells were sorted in the SY3200 cell sorter (Synergy). Cells were kept in DMEM Glutamax F-12 media (15% FBS) with added penicillin/streptomycin (100 IU/mL) and puromycin for selection (2 μg/mL). UCH-L1 KD was confirmed by Western Blot. UCH-L1 KD and scrambled cells were frozen one week after sorting and, when thawed, used for maximum of 3 weeks. UCH-$L1^{WT}$, vector and UCH-$L1^{220S}$ were kindly provided by Prof.. Peter Lansbury [60]. The mutant C220S was generated by PCR mutagenesis as described in Ref. [17].

3.2. Western blots

Cell lysates were diluted in Laemmli sample buffer (100 mMTris–HCl, 2% SDS, 10% glycerol, 0.1% bromophenol blue) containing 5% β-mercaptoethanol. After heating at 95 °C, proteins were separated by SDS-PAGE and transferred onto PVDF membranes. Membranes were blocked with 5% non-fat milk and detection of individual proteins was carried out by blotting with specific primary antibody against UCH-L1 (Santa Cruz, 1:5000), Mfn2 (Abcam, 1:1000), Mfn1

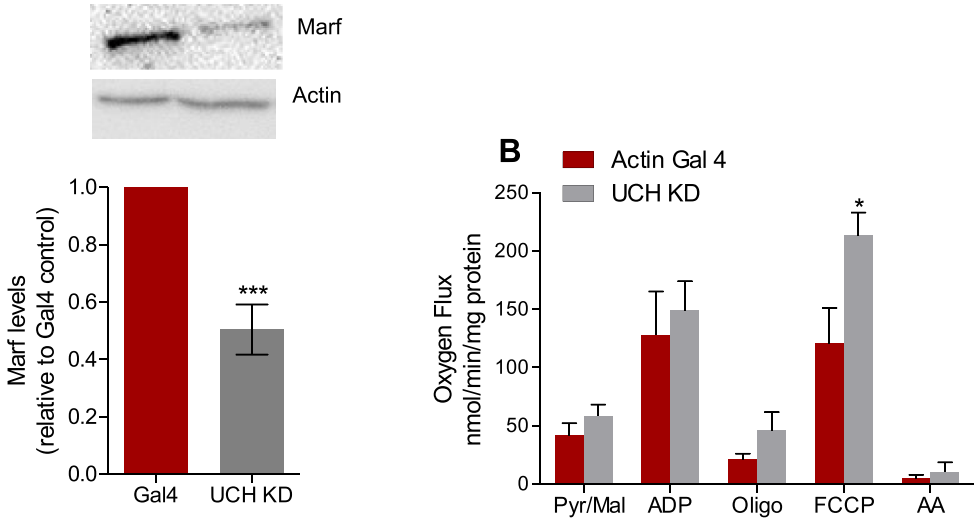

Fig. 7. UCHL-1 knockdown in *D. melanogaster* reduces Marf levels and increases maximum oxygen flux. (A) Marf levels from whole body lysate from *Drosophila* with UCH knockdown or Actin Gal 4 control vetor. (B) Representative oxygen consumption chart from mitochondria isolated from Actin Gal 4 or UCH KD flies at basal (pyruvate/malate) and stimulated by ADP 2 μM, Oligomycin 2 μM, and FCCP 1.5 μM. Antimycin (2 μM) was used to block mitochondrial respiration at the end of the assay. (C) O_2 flux calculated in the presence of each respiration modulator. $^*p < 0.05$ *vs.* actin Gal4; $^{***}p < 0.001$ *vs.* actin Gal4.

(Novus Biological, 1:1000), and VDAC (Abcam, 1:1000). Chemiluminescence detection using a secondary peroxidase-linked anti-rabbit (1:10,000) or anti-mouse (1:10,000) and a detection system from Pierce KLP (Rockford, IL, USA) was performed. Bands were analyzed in Image J.

3.3. Aequorin measurements of Ca^{2+} concentrations

Cells stably expressing scramble or UCH-L1 shRNA grown on 13-mm round glass coverslips at 50% confluence were infected with adenoviruses carrying cytosolic (cyt) or mitochondrial (mt) AEQ as reported in Ref. [72]. Cyt and mtAEQ reconstitution, measurement, and calibration were performed as described previously [43,73], in KRB (125 mM NaCl, 5 mM KCl, 1 mM Na_3PO_4, 1 mM $MgSO_4$, 5.5 mM glucose, 20 mM Hepes, pH 7.4) supplemented with 10 mM EGTA. Calcium uptake was stimulated with the addition of ATP (0.2 mM).

3.4. Confocal analysis of mitochondrial morphology

Live SH-SY5Y cells were transfected with scramble or UCH-L1 shRNA and co-transfected mitochondrial dsRed, using Lipofectamin 2000 (Invitrogen) diluted in Opt-MEM (Thermo Fisher), and were imaged using a Zeiss LSM 710 microscope with a ×63 oil immersion objective and 543-nm helium-neon laser with a 650- to 710-nm bandpass filter. Image J 1.41° software distinguished mitochondrial structures to analyze morphological characteristics. Length was calculated using the major axes of the ellipse equivalent to a mitochondrion and form factor measured the degree of branching (FF; perimeter^2/4π*area).

3.5. Electron microscopy

Neuroblastoma SH-SY5Y cells of the indicated background were fixed with 1.25% (vol/vol) glutaraldehyde in 0.1 M sodium cacodylate at pH 7.4 for 1 h at room temperature. Thin sections were imaged on a Tecnai-20 electron microscope (Philips-FEI). Morphometric measurements were carried out using ImageJ (National Institutes of Health). For calculations of mitochondria-ER distance, 200 images per condition were considered and a minimum distance of ER located in a 30- or 20-nmn radius from the considered mitochondrion was computed [42,43].

3.6. Cellular oxygen consumption

An hour before oxygen consumption measurements, cell media was replaced by assay media (2 mM glucose, 0.8 mM Mg^{2+}, 1.8 mM Ca^{2+}, 143 mM NaCl, 5.4 mM KCl, 0.91 mM, NaH_2PO_4, and 15 mg/mL Phenol red) for 120 min at 37 °C (no CO_2) before loading into the Seahorse Bioscience XF24 extracellular analyzer [74]. The ports of the cartridge containing oxygen probes were loaded with compounds to be injected during the assay (50μL/port) and the cartridge was calibrated.

Basal respiration was recorded for 30 min, at approximately 5 min intervals until system stabilization. FCCP (Carbonyl cyanide-4-phenylhydrazone) was used at a final concentration of 2 μM and injected with sodium pyruvate (Sigma) at a final concentration of 5 mM. Oligomycin and antimycin were used at final concentrations of 2 and 4 μM, respectively. All respiratory modulators were used at ideal concentrations titrated during preliminary experiments (not shown) and oxygen consumption rates were recorded for up to 15 min due the toxicity of these compounds. All the OCR values were subtracted from the lowest antimycin OCR.

3.7. Complex I activity assay

Mitochondrial complex I enzyme activity was measured using Abcam's complex I enzyme activity microplate assay kit by following the oxidation of reduced nicotinamide adenine dinucleotide (NADH) to oxidized NAD^+ and the simultaneous reduction of a dye which leads to increased absorbance at OD = 450 nm.

3.8. Complex II activity assay

Complex II activity was assessed in cell homogenates as described in Spinazzi et al. (2012) [75], with some modifications. Briefly, cell homogenates were incubated in phosphate buffer (25 mM, pH 7.5) containing fatty acid free bovine serum albumin (3 mg mL^{-1}), antimycin A (1 μg mL^{-1}), succinate (20 μM) and 2,6-dichlorophenolindolphenol (80 μM). The activity was followed as the decrease in 2,6-dichlorophenolindolphenol absorbance after decylubiquinone (50 μM) addition at 600 nm (ε = 19.1 $mmol^{-1}$ cm^{-1}) and corrected by total protein content.

3.9. Immunostaining and structured illumination microscopy

SH-SY5Y cells were seeded at 30% density on number 1.5 coverslips (Marienfeld, Lauda-Konigshfen, Germany). After 24 h, cells were transfected with vector, UCH-L1^{WT} or UCH-L1^{C220S}. Forty-eight hours after transfection, the cells were fixed using 4% paraformaldehyde, followed by permeabilization (Triton X 0.1%), blocking (BSA 10%), and primary (Mfn2 and UCH-L1 antibodies, 1:500, Abcam and Santa Cruz, respectively) and secondary antibodies (Anti-Mouse-Alexa Fluor-488 and Anti-Rabbit-Alexa Fluor-647, 1:1,000, respectively, Life Technologies). Last, samples were mounted with Fluoromount-G (SouthernBiotech). Thin (0.163 μm) *z*-stacks of high-resolution images were collected using a 63× oil immersion objective (numerical aperture, 1.4), in five rotations on an ELYRA PS.1 microscope (Zeiss, Jena, Germany). Images were then reconstructed using ZEN software (Zeiss) based on the structured illumination algorithm developed by Ref. [76].

3.10. Drosophila stocks and procedures

Drosophila were raised under standard conditions at 25 °C on agar, cornmeal, yeast food. The *Act5C-GAL4* strain was obtained from the Bloomington *Drosophila* Stock Center (Bloomington, IN). UAS-UCHL1 RNAi lines were obtained from VDRC Stock Center. UAS UCHL1 KD line was crossed with an Act5C-Gal4 driver line to ubiquitously activate RNAi of UCHL1.

Mitochondria were extracted from whole flies by differential centrifugation. Each sample was homogenized using a Dounce glass-glass potter and a loose-fitting pestle in a mannitol-sucrose buffer (225 mM mannitol, 75 mM sucrose, 5 mM Hepes, 0.1 mM EGTA, pH 7.4) supplemented with 2% BSA. Samples were then centrifuged at 1500×*g* at 4 °C for 6 min. The pellet was discarded by filtering the sample through a fine mesh, and the supernatant was centrifuged at 7000×*g* at 4 °C for 6 min. The resulting pellet was resuspended in mannitol-sucrose buffer without BSA before being centrifuged at 7000×*g* under the same conditions as above and resuspended in a small volume of mannitol-sucrose buffer. Protein concentration was measured using the Biuret test.

Rates of mitochondrial respiration were measured using the Oxytherm system (Hansatech) with magnetic stirring and thermostatic control maintained at 25 °C. Isolated *Drosophila* mitochondria (1 mg/ml) were incubated in 120 mM KCl, 5 mM P_i-Tris, 3 mM Hepes, 1 mM EGTA, 1 mM $MgCl_2$, pH 7.2, and additions were made as indicated in the figure legends. O_2 consumption was calculated according to the slope of the registered graph, and plotted as ng atoms O_2 x min^{-1} x mg^{-1}.

Declaration of competing interest

The authors declare no conflict of interest.

Acknowledgements

We would like to thank Professor. Peter Lansbury and Dr. Robin Meray for the donation and assistance with the UCH-L1 plasmids. We are

also deeply grateful to Professor Luca Scorrano for the insightful discussions and Professor Daniel Dagan for the critical reading of the manuscript. We thank Francesco Boldrin from the Electron Microscopy Facility at Padova University and Camille Caldeira from Sao Paulo University for the help and technical support and MSc. João Victor Cabral Costa for the art work. O.S.S. is funded by an R01 grant from NIH-NIDDK (5R01DK099618-05). F.M.C was supported by CAPES-CNPq / Brazil and EMBO (ASTF 584-2015). M.G. is funded by CARIPARO Starting Grant 2016 AIFbiol, Unipd STARS Consolidator grant "Featuring a new class of Interface Regulators". E.Z. was funded by the Italian Ministry of Health "Ricerca Finalizzata" (GR-2011-02351151). A. J.K. is funded by Fundação de Amparo à Pesquisa do Estado de São Paulo (FAPESP) grant 13/07937-8. P.K. is funded by FAPESP (Grant 2015/25862-0).

Appendix A. Supplementary data

Supplementary data to this article can be found online at https://doi.org/10.1016/j.redox.2020.101676.

References

[1] S. Selvaraj, S. Piramanayagam, Impact of gene mutation in the development of Parkinson's disease, Genes Dis. 27 (2019) 120–128.
[2] C. Klein, A. Westenberger, Genetics of Parkinson's disease, Cold Spring Harb. Perspect. Med. 2 (2012) a008888.
[3] M.S. Parihar, A. Parihar, M. Fujita, M. Hashimoto, P. Ghafourifar, Mitochondrial association of alpha-synuclein causes oxidative stress, Cell. Mol. Life Sci. 65 (2008) 1272–1284.
[4] W.W. Smith, H. Jiang, Z. Pei, Y. Tanaka, H. Morita, A. Sawa, V.L. Dawson, T. M. Dawson, C.A. Ross, Endoplasmic reticulum stress and mitochondrial cell death pathways mediate A53T mutant alpha-synuclein-induced toxicity, Hum. Mol. Genet. 14 (2015) 3801–3811.
[5] X. Wang, K. Becker, N. Levine, M. Zhang, A.P. Lieberman, D.J. Moore, J. Ma, Pathogenic alpha-synuclein aggregates preferentially bind to mitochondria and affect cellular respiration, Acta Neuropathol. Commun. 14 (2019) 41.
[6] M.W. Dodson, M. Guo, Pink1, Parkin, DJ-1 and mitochondrial dysfunction in Parkinson's disease, Curr. Opin. Neurobiol. 17 (2007) 331–337.
[7] S. Geisler, K.M. Holmström, D. Skujat, F.C. Fiesel, O.C. Rothfuss, P.J. Kahle, W. Springer, PINK1/Parkin mediated mitophagy is dependent on VDAC and p62/SQSTM1, Nat. Cell Biol. 12 (2010) 119–131.
[8] C. Vives-Bauza, C. Zhou, Y. Huang, M. Cui, R.L. de Vries, J. Kim, J. May, M. A. Tocilescu, W. Liu, H.S. Ko, J. Magrané, D.J. Moore, V.L. Dawson, R. Grailhe, T. M. Dawson, C. Li, K. Tieu, S. Przedborski, PINK1-dependent recruitment of Parkin to mitochondria and mitophagy, Proc. Natl. Acad. Sci. U. S. A. 107 (2010) 378–383.
[9] N. Matsuda, S. Sato, K. Shiba, K. Okatsu, K. Saisho, C.A. Gautier, Y.S. Sou, S. Saiki, S. Kawajiri, F. Sato, M. Kimura, M. Komatsu, N. Hattori, K. Tanaka, PINK1 stabilized by mitochondrial depolarization recruits Parkin to damaged mitochondria and activates latent Parkin for mitophagy, J. Cell Biol. 189 (2010) 211–221.
[10] M.K. McCoy, M.R. Cookson, DJ-1 regulation of mitochondrial function and autophagy through oxidative stress, Autophagy 7 (2011) 531–532.
[11] M.E. Gegg, J.M. Cooper, K.Y. Chau, M. Rojo, A.H. Schapira, J.W. Taanman, Mitofusin 1 and mitofusin 2 are ubiquitinated in a PINK1/parkin-dependent manner upon induction of mitophagy, Hum. Mol. Genet. 19 (2010) 4861–4870.
[12] Jaime M. Ross, Lars Olson, Giuseppe Coppotelli, Mitochondria and ubiquitin Proteasome system dysfunction in ageing and disease: two sides of the same coin? Int. J. Mol. Sci. 16 (2015) 19458–19476.
[13] P. Bragoszewski, M. Turek, A. Chacinska, Control of mitochondrial biogenesis and function by the ubiquitin-proteasome system, Open Biol. 7 (2017) 170007.
[14] E. Leroy, R. Boyer, G. Auburger, B. Leube, G. Ulm, E. Mezey, G. Harta, M. J. Brownstein, S. Jonnalagada, T. Chernova, A. Dehejia, C. Lavedan, T. Gasser, P. J. Steinbach, K.D. Wilkinson, M.H. Polymeropoulos, The ubiquitin pathway in Parkinson's disease, Nature 395 (1998) 451–452.
[15] C.N. Larsen, J.S. Price, K.D. Wilkinson, Substrate binding and catalysis by ubiquitin C-terminal hydrolases: identification of two active site residues, Biochemistry 35 (1996) 6735–6744.
[16] C.N. Larsen, B.A. Krantz, K.D. Wilkinson, Substrate specificity of deubiquitinating enzymes: ubiquitin C-terminal hydrolases, Biochemistry 37 (1998) 3358–3368.
[17] Z. Liu, R.K. Meray, T.N. Grammatopoulos, R.A. Fredenburg, M.R. Cookson, Y. Liu, T. Logan, P.T. Lansbury Jr., Membrane-associated farnesylated UCH-L1 promotes alpha-synuclein neurotoxicity and is a therapeutic target for Parkinson's disease, Proc. Natl. Acad. Sci. Unit. States Am. 106 (2009) 4635–4640.
[18] K.D. Wilkinson, K.M. Lee, S. Deshpande, P. Duerksen-Hughes, J.M. Boss, J. Pohl, The neuron-specific protein PGP 9.5 is a ubiquitin carboxyl-terminal hydrolase, Science 246 (1989) 670–673.
[19] J.F. Doran, P. Jackson, P.A. Kynoch, R.J. Thompson, Isolation of PGP 9.5, a new human neurone-specific protein detected by high-resolution two-dimensional electrophoresis, J. Neurochem. 40 (1983) 1542–1547.
[20] J.E. McKeon, D. Sha, L. Li, L.S. Chin, Parkin-mediated K63-polyubiquitination targets ubiquitin C-terminal hydrolase L1 for degradation by the autophagy-lysosome system, Cell. Mol. Life Sci. 72 (2015) 1811–1824.
[21] M. Picard, K. White, D.M. Turnbull, Mitochondrial morphology, topology, and membrane interactions in skeletal muscle: a quantitative three-dimensional electron microscopy study, J. Appl. Physiol. 114 (2013) 161–171, 1985.
[22] A. Tanaka, M.M. Cleland, S. Xu, D.P. Narendra, D.F. Suen, M. Karbowski, R. J. Youle, Proteasome and p97 mediate mitophagy and degradation of mitofusins induced by Parkin, J. Cell Biol. 191 (2010) 1367–1380.
[23] J. Lavie, H. De Belvalet, S. Sonon, A.M. Ion, E. Dumon, S. Melser, D. Lacombe, J. W. Dupuy, C. Lalou, G. Bénard, Ubiquitin-dependent degradation of mitochondrial proteins regulates energy metabolism, Cell Rep. 23 (2018) 2852–2863.
[24] F. Atouf, P. Czernichow, R. Scharfmann, Expression of neuronal traits in pancreatic beta cells. Implication of neuron-restrictive silencing factor/repressor element silencing transcription factor, a neuron-restrictive silencer, J. Biol. Chem. 272 (1997) 1929–1934.
[25] M.D. Lopez-Avalos, V.F. Duvivier-Kali, G. Xu, S. Bonner-Weir, A. Sharma, G. C. Weir, Evidence for a role of the ubiquitin-proteasome pathway in pancreatic islets, Diabetes 55 (2006) 1223–1231.
[26] S. Costes, C.J. Huang, T. Gurlo, M. Daval, A.V. Matveyenko, R.A. Rizza, A.E. Butler, P.C. Butler, β-cell dysfunctional ERAD/ubiquitin/proteasome system in type 2 diabetes mediated by islet amyloid polypeptide-induced UCH-L1 deficiency, Diabetes 60 (2011) 227–238.
[27] A. Mourier, E. Motori, T. Brandt, M. Lagouge, I. Atanassov, A. Galinier, G. Rappl, S. Brodesser, K. Hultenby, C. Dieterich, N.G. Larsson, Mitofusin 2 is required to maintain mitochondrial coenzyme Q levels, J. Cell Biol. 208 (2015) 429–442.
[28] H. Chen, S.A. Detmer, A.J. Ewald, E.E. Griffin, S.E. Fraser, D.C. Chan, Mitofusins Mfn1 and Mfn2 coordinately regulate mitochondrial fusion and are essential for embryonic development, J. Cell Biol. 160 (2003) 189–200.
[29] A. Rakovic, A. Grünewald, J. Kottwitz, N. Brüggemann, P.P. Pramstaller, K. Lohmann, C. Klein, Mutations in PINK1 and Parkin impair ubiquitination of Mitofusins in human and fibroblasts, PloS One 6 (2011), e16746.
[30] E. Ziviani, R.N. Tao, A.J. Whitworth, Drosophila parkin requires PINK1 for mitochondrial translocation and ubiquitinates mitofusin, Proc. Natl. Acad. Sci. U. S. A. 107 (2010) 5018–5023.
[31] A. Santel, M.T. Fuller, Control of mitochondrial morphology by a human mitofusin, J. Cell Sci. 114 (2001) 867–874.
[32] M. Rojo, F. Legros, D. Chateau, A. Lombès, Membrane topology and mitochondrial targeting of mitofusins, ubiquitous mammalian homologs of the transmembrane GTPase Fzo, J. Cell Sci. 115 (2002) 1663–1674.
[33] D. Bach, S. Pich, F.X. Soriano, N. Vega, B. Baumgartner, J. Oriola, J.R. Daugaard, J. Lloberas, M. Camps, J.R. Zierath, R. Rabasa-Lhoret, H. Wallberg-Henriksson, M. Laville, M. Palacín, H. Vidal, F. Rivera, M. Brand, A. Zorzano, Mitofusin 2 determines mitochondrial network architecture and mitochondrial metabolism. A novel regulatory mechanism altered in obesity, J. Biol. Chem. 278 (2003) 17190–17197.
[34] O.M. de Brito, L. Scorrano, Mitofusin-2 regulates mitochondrial and endoplasmic reticulum morphology and tethering: the role of Ras, Mitochondrion 9 (2009) 222–226.
[35] W. Yue, Z. Chen, H. Liu, C. Yan, M. Chen, D. Feng, C. Yan, H. Wu, L. Du, Y. Wang, J. Liu, X. Huang, L. Xia, L. Liu, X. Wang, H. Jin, J. Wang, Z. Song, X. Hao, Q. Chen, A small natural molecule promotes mitochondrial fusion through inhibition of the deubiquitinase USP30, Cell *Res* 24 (2014) 482–496.
[36] Y. Wang, M. Serricchio, M. Jauregui, R. Shanbhag, T. Stoltz, C.T. Di Paolo, P. K. Kim, G.A. McQuibban, Deubiquitinating enzymes regulate PARK2-mediated mitophagy, Autophagy 11 (2015) 595–606.
[37] T. Cornelissen, D. Haddad, F. Wauters, C. Van Humbeeck, W. Mandemakers, B. Koentjoro, C. Sue, K. Gevaert, B. De Strooper, P. Verstreken, W. Vandenberghe, The deubiquitinase USP15 antagonizes Parkin-mediated mitochondrial ubiquitination and mitophagy, Hum. Mol. Genet. 23 (2014) 5227–5242.
[38] J. Chakraborty, S. von Stockum, E. Marchesan, F. Caicci, V. Ferrari, A. Rakovic, C. Klein, A. Antonini, L. Bubacco, E. Ziviani, USP14 inhibition corrects an *in vivo* model of impaired mitophagy, EMBO Mol. Med. 10 (2018), e9014 pii.
[39] G. Csordás, C. Renken, P. Várnai, L. Walter, D. Weaver, K.F. Buttle, T. Balla, C. A. Mannella, G. Hajnóczky, Structural and functional features and significance of the physical linkage between ER and mitochondria, J. Cell Biol. 174 (2006) 915–921.
[40] M. Giacomello, L. Pellegrini, The coming of age of the mitochondria-ER contact: a matter of thickness, Cell Death Differ. 23 (2016) 1417–1427.
[41] G. Csordás, P. Várnai, T. Golenár, S. Roy, G. Purkins, T.G. Schneider, T. Balla, G. Hajnóczky, Imaging interorganelle contacts and local calcium dynamics at the ER-mitochondrial interface, Mol. Cell. 39 (2010) 121–132.
[42] D. Naon, M. Zaninello, M. Giacomello, T. Varanita, F. Grespi, S. Lakshminaranayan, A. Serafini, M. Semenzato, S. Herkenne, M.I. Hernández-Alvarez, A. Zorzano, D. De Stefani, G.W. Dorn 2nd, L. Scorrano, Critical reappraisal confirms that Mitofusin 2 is an endoplasmic reticulum-mitochondria tether, P*roc. Natl. Acad. Sci. U. S. A.* 1**13** (2016) 11249–11254.
[43] O.M. de Brito, L. Scorrano, Mitofusin 2 tethers endoplasmic reticulum to mitochondria, Nature 456 (2008) 605–610.
[44] A. Ainbinder, S. Boncompagni, F. Protasi, R.T. Dirksen, Role of Mitofusin-2 in mitochondrial localization and calcium uptake in skeletal muscle, Cell *Calcium* 57 (2015) 14–24.

[45] R. Filadi, E. Greotti, G. Turacchio, A. Luini, T. Pozzan, P. Pizzo, Mitofusin 2 ablation increases endoplasmic reticulum-mitochondria coupling, Proc. Natl. Acad. Sci. U. S. A. 112 (2015) E2174–E2181.
[46] P. Cosson, A. Marchetti, M. Ravazzola, L. Orci, Mitofusin-2 independent juxtaposition of endoplasmicc reticulum and mitochondria: an ultrastructural study, PloS One 7 (2012), e46293.
[47] G. Szabadkai, A.M. Simoni, M. Chami, M.R. Wieckowski, R.J. Youle, R. Rizzuto, Drp-1-dependent division of the mitochondrial network blocks intraorganellar Ca^{2+} waves and protects against Ca^{2+}-mediated apoptosis, Mol. Cell. 16 (2004) 59–68.
[48] M.D. Brand, The proton leak across the mitochondrial inner membrane, Biochim. Biophys. Acta 1018 (1990) 128–133.
[49] M.H. Barros, B. Bandy, E.B. Tahara, A.J. Kowaltowski, Higher respiratory activity decreases mitochondrial reactive oxygen release and increases life span in Saccharomyces cerevisiae, J. Biol. Chem. 279 (2004) 49883–49888.
[50] M. Liesa, O.S. Shirihai, Mitochondrial dynamics in the regulation of nutrient utilization and energy expenditure, Cell Metabol. 17 (2013) 491–506.
[51] J. Pfleger, M. He, M. Abdellatif, Mitochondrial complex II is a source of the reserve respiratory capacity that is regulated by metabolic sensors and promotes cell survival, Cell Death Dis. 6 (2015), e1835.
[52] C. Sauvanet, S. Duvezin-Caubet, J.P. di Rago, M. Rojo, M. Rojo, Energetic requirements and bioenergetic modulation of mitochondrial morphology and dynamics, Semin. Cell Dev. Biol. 21 (2010) 558–565.
[53] A. Zorzano, M.I. Hernández-Alvarez, D. Sebastián, J.P. Muñoz, Mitofusin 2 as a driver that controls energy metabolism and insulin signaling, Antioxidants Redox Signal. 22 (2015) 1020–1031.
[54] E. Schrepfer, L. Scorrano, Mitofusins, from mitochondria to metabolism, Mol. Cell. 61 (2016) 683–694.
[55] S. Pich, D. Bach, P. Briones, M. Liesa, X. Camps, M. Testar, M. Palacin, A. Zorzano, The Charcot-Marie-Tooth type 2A gene product, Mfn2, up-regulates fuel oxidation through expression of OXPHOS system, Hum. Mol. Genet. 14 (2005) 1405–1415.
[56] M. Kawalec, A. Boratyńska-Jasińska, M. Beręsewicz, D. Dymkowska, K. Zabłocki, B. Zabłocka, Mitofusin 2 deficiency affects energy metabolism and mitochondrial biogenesis in MEF cells, PloS *One* 10 (2015), e0134162.
[57] K. Mahdaviani, I.Y. Benador, S. Su, R.A. Gharakhanian, L. Stiles, K.M. Trudeau, M. Cardamone, V. Enríquez-Zarralanga, E. Ritou, T. Aprahamian, M.F. Oliveira, B. E. Corkey, V. Perissi, M. Liesa, O.S. Shirihai, Mfn2 deletion in brown adipose tissue protects from insulin resistance and impairs thermogenesis, EMBO Rep. 18 (2017) 1123–1138.
[58] C. Das, Q.Q. Hoang, C.A. Kreinbring, S.J. Luchansky, R.K. Meray, S.S. Ray, P. T. Lansbury, D. Ringe, G.A. Petsko, Structural basis for conformational plasticity of the Parkinson's disease-associated ubiquitin hydrolase UCH-L1, Proc. Natl. Acad. Sci. U. S. A. 103 (2006) 4675–4680.
[59] D.A. Boudreaux, T.K. Maiti, C.W. Davies, C. Das, Ubiquitin vinyl methyl ester binding orients the misaligned active site of the ubiquitin hydrolaseUCHL1 into productive conformation, Proc. Natl. Acad. Sci. U S A 107 (20) (2010 May 18) 9117–9122.
[60] Y. Liu, L. Fallon, H.A. Lashuel, Z. Liu, P.T. Lansbury Jr., The UCH-L1 gene encodes two opposing enzymatic activities that affect alpha-synuclein degradation and Parkinson's disease susceptibility, Cell 111 (2002) 209–218.
[61] J.S. Bett, M.S. Ritorto, R. Ewan, E.G. Jaffray, S. Virdee, J.W. Chin, A. Knebel, T. Kurz, M. Trost, M.H. Tatham, R.T. Hay, Ubiquitin C-terminal hydrolases cleave isopeptide- and peptide-linked ubiquitin from structured proteins but do not edit ubiquitin homopolymers, Biochem. J. 466 (2015) 489–498.
[62] H. Osaka, Y.L. Wang, K. Takada, S. Takizawa, R. Setsuie, H. Li, Y. Sato, K. Nishikawa, Y.J. Sun, M. Sakurai, T. Harada, Y. Hara, I. Kimura, S. Chiba, K. Namikawa, H. Kiyama, M. Noda, S. Aoki, K. Wada, Ubiquitin carboxy-terminal hydrolase L1 binds to and stabilizes monoubiquitin in neuron, Hum. Mol. Genet. 12 (2003) 1945–1958.
[63] B. Bingol, J.S. Tea, L. Phu, M. Reichelt, C.E. Bakalarski, Q. Song, O. Foreman, D. S. Kirkpatrick, M. Sheng, The mitochondrial deubiquitinase USP30 opposes parkin-mediated mitophagy, Nature 510 (2014) 370–375.
[64] J.W. Harper, A. Ordureau, J.M. Heo, Building and decoding ubiquitin chains for mitophagy, Nat. Rev. Mol. Cell Biol. 19 (2018) 93–108.
[65] S. Von Stockum, A. Sanchez-Martinez, S. Corrà, J. Chakraborty, E. Marchesan, L. Locatello, C. Da Rè, P. Cusumano, F. Caicci, V. Ferrari, R. Costa, L. Bubacco, M. B. Rasotto, I. Szabo, A.J. Whitworth, L. Scorrano, E. Ziviani, Inhibition of the deubiquitinase USP8 corrects a Drosophila PINK1 model of mitochondria dysfunction, Life Sci. Alliance 2 (2019), e201900392 pii.
[66] H.H. Tran, S.N.A. Dang, T.T. Nguyen, A.M. Huynh, L.M. Dao, K. Kamei, M. Yamaguchi, T.T.P. Dang, Drosophila ubiquitin C-terminal hydrolase knockdown model of Parkinson's disease, Sci. Rep. 8 (2018) 4468.
[67] C. Greggio, P. Jha, S.S. Kulkarni, S. Lagarrigue, N.T. Broskey, M. Boutant, X. Wang, S. Conde Alonso, E. Ofori, J. Auwerx, C. Cantó, F. Amati, Enhanced respiratory chain supercomplex formation in response to exercise in human skeletal muscle, Cell Metabol. 7 (2017) 301–311.
[68] H. Lemieux, P.U. Blier, E. Gnaiger, Remodeling pathway control of mitochondrial respiratory capacity by temperature in mouse heart: electron flow through the Q-junction in permeabilized fibers, Sci. Rep. 7 (2017) 2840.
[69] P. Bishop, D. Rocca, J.M. Henley, Ubiquitin C-terminal hydrolase L1 (UCH-L1): structure, distribution and roles in brain function and dysfunction, Biochem. J. **473** (2016) 2453–2462.
[70] F.L. Tang, W. Liu, J.X. Hu, J.R. Erion, J. Ye, L. Mei, W.C. Xiong, VPS35 deficiency or mutation causes dopaminergic neuronal loss by impairing mitochondrial fusion and function, Cell Rep. 12 (2015) 1631–1643.
[71] Y. Yang, L.J. Xue, X. Xue, Z. Ou, T. Jiang, Y.D. Zhang, MFN2 ameliorates cell apoptosis in a cellular model of Parkinson's disease induced by rotenone, Exp. Ther. Med. 16 (2018) 3680–3685.
[72] A. Raffaello, D. De Stefani, D. Sabbadin, E. Teardo, G. Merli, A. Picard, V. Checchetto, S. Moro, I. Szabò, R. Rizzuto, The mitochondrial calcium uniporter is a multimer that can include a dominant-negative pore-forming subunit, EMBO J. 3217 (2013) 2362–2376.
[73] D. Larrea, M. Pera, A. Gonnelli, R. Quintana-Cabrera, H.O. Akman, C. Guardia-Laguarta, K.R. Velasco, E. Area-Gomez, F. Dal Bello, D. De Stefani, R. Horvath, M. E. Shy, E.A. Schon, M. Giacomello, MFN2 mutations in Charcot-Marie-Tooth disease alter mitochondria-associated ER membrane function but do not impair bioenergetics, Hum. Mol. Genet. 28 (2019) 1782–1800.
[74] M. Wu, A. Neilson, A.L. Swift, R. Moran, J. Tamagnine, D. Parslow, S. Armistead, K. Lemire, J. Orrell, J. Teich, S. Chomicz, D.A. Ferrick, Multiparameter metabolic analysis reveals a close link between attenuated mitochondrial bionergetic function and enhanced glycolysis dependency in tumor cells, Am. J. Physiol. 292 (2007) C125–C136.
[75] M. Spinazzi, A. Casarin, V. Pertegato, L. Salviati, C. Angelini, Assessment of mitochondrial respiratory chain enzymatic activities on tissues and cultured cells, Nat. Protoc. 7 (2012) 1235–1246.
[76] R. Heintzmann, C.G. Cremer, Laterally modulated excitation microscopy: improvement of resolution by using a diffraction grating, Proc. SPIE 3568 (1999) 185–196.